Magnon cat states induced by photon parametric coupling

Da-Wei Liu, Ying Wu, and Liu-Gang Si*

School of Physics, Huazhong University of Science and Technology, Wuhan 430074, People's Republic of China

(Received 9 August 2023; revised 7 November 2023; accepted 18 March 2024; published 8 April 2024)

Cat state, is not only interesting for testing the fundamentals of quantum mechanics, but also for wide applications ranging from fault-tolerant quantum computation to quantum metrology. Here, we propose a scheme to generate the magnon cat state by the indirect magnon nonlinearity. We show that the effective two-magnon loss process can be induced by the photon parametric coupling, steering the magnon into the cat-state manifold. In our work, the size of the magnon cat state can be easily adjusted, and the large-size cat state can be generated with high fidelity. At the same time, the speed of cat-state generation can be greatly improved by enhancing the photon-magnon interaction with maintaining a larger size of cat state. Further, we find that the effective two-magnon loss process can strongly suppress the decoherence of the environment under appropriate parameter conditions. The lifetime of the magnon cat state can be expected to be $t \sim 3$ μs under the current experimental techniques. This work provides a proposal for the preparation of nonclassical states of magnons without the direct magnon nonlinearity, which is meaningful for the development of quantum technology in the future.

DOI: 10.1103/PhysRevApplied.21.044018

I. INTRODUCTION

Cat state, as a pure quantum effect, was proposed by Schrödinger [1], which describes the quantum superposition of macroscopic objects. In quantum optics, the coherent state, with the minimum uncertainty, is regarded as a quasiclassical state. Therefore, the superposition of two coherent states $\mathcal{N}(|\alpha\rangle + e^{i\phi}|-\alpha\rangle)$ is defined as the cat state [2–6], where $\mathcal{N}$ is the normalization coefficient and α is the coherent amplitude. It will be divided into the even and odd cat state when $\phi = 0$ and $\phi = \pi$, respectively [6,7]. The cat states not only reveal the essence of quantum theory [8–13], but also play a role in understanding the transition between macroscopic and microscopic worlds in quantum theory [14,15]. Meanwhile, they also have wide applications in various fields, such as fault-tolerant quantum computation [16–19] and metrology [20,21]. In the past few decades, a number of methods have been used to prepare cat states [22–44]. Through Rabi [42] or radiation pressure interaction [34], the transient entangled state can be prepared by unitary time evolution, then one can obtain the cat state by selective quantum measurements. On the other hand, by engineering a nonlinear loss [45,46], the stable cat state can be decisively generated, which can effectively suppress the dephase. However, the preparation and stability of cat states still remain a challenge due to the inevitable decoherence of the environment. So far, the cat state has been observed experimentally in various physical systems [47], i.e., electronic [48–50], photonic [14,51], and atomic or molecular systems [15,52].

Hybrid quantum systems play a role in the exploration of various quantum effects [53,54]. A cavity magnon system, as an alternative type of hybrid system, has attracted tremendous experimental [55–59] and theoretical attention [60–64]. Magnons, similar to phonons, are a kind of quasiparticle of the collective spin excitations in ordered magnets. In ferromagnetic materials and microwave ferrites, yttrium iron garnet (YIG) is favored by researchers due to its unique advantages, such as long lifetimes, low dissipation rate [55,65–69], tunable frequency, and convenient operation. On the other hand, through magneto-optical [70–73], magnetostriction effects [73,74] and magnetic dipoles [75–78], magnons can interact directly with optical photons, phonons and microwaves, in which the coupling between photons and magnons can reach the strong coupling regime [67–69] benefiting from the high spin density of YIG. At the same time, the indirect coupling between the magnon and superconducting qubit can be achieved through the virtual photon process that has also been experimentally reported [79], and the scheme of direct coupling between the magnon and superconducting qubit has also been proposed theoretically [80]. Similar to photonic systems, many phenomena have been reported in magnonic systems, such as bistability [75], magnon laser [81–83], antibunching [84], squeezed state [85–87], and cat state [88–90].

Recently, the schemes of preparing the cat state relying on the anisotropy of the magnet in ferromagnetic insulators [88] and projecting measurement the optical (qubit) mode

*Corresponding author. siliugang@hust.edu.cn

via magnon-photon entanglement [89] or magnon-qubit entanglement [80] have been proposed. However, these schemes directly require the nonlinearity of the magnons, i.e., the squeezed terms induced by anisotropy shape and the terms analogous to the radiation pressure in optomechanics. A natural question is whether the indirect magnon nonlinearity can induce the generation of magnon cat states.

Here, we propose another scheme to generate the magnon cat state by the indirect magnon nonlinearity. In our scheme, the photon parametric down-conversion process is transferred to the magnon, thus forming an effective two-magnon process. The odd and even cat state can be generated with high fidelity and large size by the two-magnon loss. We discuss the influence of the driving phase on the fidelity of the odd and even cat state and find that the fidelity will have an evident perturbation by the phase. At the same time, the speed of cat-state generation can be greatly improved by enhancing the photon-magnon interaction with maintaining a larger size of the cat state. Further, we find that the single-magnon dissipation can be strongly suppressed by the two-magnon loss when the single-magnon dissipation is much smaller than the effective two-magnon loss. It ensures that the even and odd magnon cat states can be generated with high fidelity. Finally, thanks to the low dissipation of the magnon, the lifetime of the cat state is expect to be $t \sim 3$ μs. Compared with the previous scheme that requires a direct magnon nonlinearity, our scheme transfers the requirement of the magnon mode to the microwave photon mode, which to some extent improves the feasibility of the experiment and provides an alternative solution for the generation of the magnon cat state.

II. MODEL AND ANALYSIS

A schematic diagram of our proposed system is depicted in Fig. 1. It consists of a pump cavity (left) and a signal cavity (right) with parametric interaction, while a YIG sphere is placed in the signal cavity. Simultaneously, an external magnetic field H is applied in the z direction, and a uniform magnon mode appears in the sphere at the resonance frequency $\omega_m = \gamma H$, where $\gamma = 2\pi \times 28$ GHz/T is the gyromagnetic ratio. The total Hamiltonian of the system is written as ($\hbar = 1$)

$$H = \omega_s a_s^\dagger a_s + \omega_p a_p^\dagger a_p + \omega_m m^\dagger m + g(a_p m^\dagger + a_p^\dagger m) + g_1(a_s^\dagger a_p^2 + a_s a_p^{\dagger 2}) + \Omega_s(a_s e^{i\omega_d t - i\phi} + a_s^\dagger e^{-i\omega_d t + i\phi}), \tag{1}$$

where $a_s(a_p)$ is the annihilation operator in the pump (signal) cavity and m is the annihilation operator of the magnon mode. g_1 is the parametric coupling strength [91–93] between the two cavities originated from the three-wave mixing process [6], and g is the photon-magnon

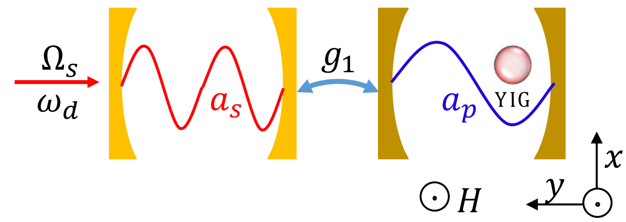

FIG. 1. Schematic diagram of magnon cat-state preparation consisting of a pump cavity (left) and signal cavity (right) with parametric interaction g_1. The YIG sphere is placed in the signal cavity, which supports the Kittel mode interacting with microwave photon modes. A uniform bias magnetic field H is applied in the z direction. The pump cavity is driven by a coherent laser with driving strength Ω_s, frequency ω_d, and initial phase ϕ.

interaction strength. The pump mode is driven by a coherent laser with driving strength Ω_s, frequency ω_d, and initial phase ϕ. We rewrite the Hamiltonian in the interaction picture by assuming that $\omega_d \approx \omega_s \approx 2\omega_m$

$$H = g(a_p m^\dagger e^{i\Delta t} + a_p^\dagger m e^{-i\Delta t}) + g_1(a_s^\dagger a_p^2 e^{i2\Delta t} + a_s a_p^{\dagger 2} e^{-i2\Delta t}) + \Omega_s(a_s e^{-i\phi} + a_s^\dagger e^{i\phi}), \tag{2}$$

where $\Delta = \omega_m - \omega_p$ is the detuning of the magnon to the signal mode. When $\Delta \gg \{g_1, g\}$, there is an effective parametric interaction between the pump mode a_s and the magnon mode m. The signal mode a_p becomes a dark mode and is always in the vacuum state under the large detuning. After time averaging and adiabaticly eliminating the signal cavity mode a_p [94,95], the effective third-order Hamiltonian is written as

$$H_{\mathrm{avg}}^{(3)} = \frac{g_1 g^2}{\Delta^2}(a_s^\dagger m^2 + a_s m^{\dagger 2}) + \Omega_s(a_s e^{-i\phi} + a_s^\dagger e^{i\phi}), \tag{3}$$

where the second-order Hamiltonian $H_{\mathrm{avg}}^{(2)} = -\frac{g_1^2}{\Delta} a_s^\dagger a_s - \frac{g^2}{\Delta} m^\dagger m$ can be eliminated by shifting the eigenfrequencies of the pump mode a_s and the magnon mode m. Meanwhile, we use the rotating-wave approximation (RWA) to omit the rapidly varying interaction terms under the condition $\Delta^2 \gg \frac{3}{4} g g_1$.

The dissipative dynamic evolution of the system is determined by the master equation

$$\dot{\rho} = -i[H_{\mathrm{avg}}^{(3)}, \rho] + (\kappa_s/2)\mathcal{L}[a_s]\rho + (\kappa_m/2)\mathcal{L}[m]\rho, \tag{4}$$

where κ_s and κ_m are the single-photon dissipation and single-magnon dissipation rates, respectively, and $\mathcal{L}[o]\rho = 2o\rho o^\dagger - o^\dagger o \rho - \rho o^\dagger o$. When $\kappa_m \ll \kappa_s$, we can adiabatically eliminate the pump cavity mode a_s to generate an effective master equation

$$\dot{\rho} = -i[H_{\text{eff}}, \rho] + (\kappa_{\text{eff}}/2)\mathcal{L}[m^2]\rho, \tag{5}$$

where $H_{\text{eff}} = J(e^{-i\phi}m^2 - m^{\dagger 2}e^{i\phi})$ is the effective Hamiltonian with effective coupling $J = i2\Omega_s g_1 g^2/\kappa_s\Delta^2$ and $\kappa_{\text{eff}} = 4g_1^2 g^4/\kappa_s\Delta^4$ is the two-magnon loss rate. The squeezed Hamiltonian and two-magnon process steer magnon into the cat-state manifold. Equation (5) has a steady-state solution for mode m that is analytically proved, while, its steady state depends only on its initial parity [45,46]. In particular, when the magnon mode m is initially in an even Fock state, its steady state is an even Schrödinger cat state with an even photon number distribution, i.e., (see Appendix A)

$$|\psi_m\rangle = \mathcal{N}_e^{-\frac{1}{2}}(|\alpha\rangle + |-\alpha\rangle), \tag{6}$$

with a normalization coefficient $\mathcal{N}_e = 2[1 + \exp(-2|\alpha|^2)]$ and the amplitude $\alpha = \sqrt{-\Omega_s\Delta^2/g_1 g^2}$. When the magnon mode m is initially in an odd Fock state, its steady state is an odd Schrödinger cat state with an odd photon-number distribution, i.e.,

$$|\psi_m\rangle = \mathcal{N}_o^{-\frac{1}{2}}(|\alpha\rangle - |-\alpha\rangle), \tag{7}$$

with a normalization coefficient $\mathcal{N}_o = 2[1 - \exp(-2|\alpha|^2)]$. For a generic initial state of mode m, its steady state will be a mixture of the even and odd Schrödinger cat state.

III. FIDELITY AND WIGNER FUNCTION

We can observe the quantum properties of the system by investigating the Wigner function. For a deterministic density matrix ρ, the Wigner function associated with it is written as

$$W(\alpha, \alpha^*) = \frac{1}{\pi^2}\int e^{\eta^*\alpha - \eta\alpha^*}\chi(\eta)d^2\eta, \tag{8}$$

where $\chi(\eta) = \text{Tr}(\rho e^{\eta m^\dagger - \eta^* m})$ is the characteristic function. When considering the magnon cat state, ρ is the reduced density matrix of the magnon from the whole system. The Wigner function of the steady-state solution of Eq. (5) is plotted in Figs. 2(a) and 2(b). We can see the two peaks with coherence amplitude $|\alpha| = 1.58$ and very obvious interference fringes (the positive and negative values of the Wigner function), showing the nonclassical nature of the magnon Schrödinger cat state.

To confirm the effectiveness of our system, we can numerically solve the master equation using the original Hamiltonian in Eq. (1) to simulate the time evolution of F as shown in Fig. 2(c). Here F is the fidelity between

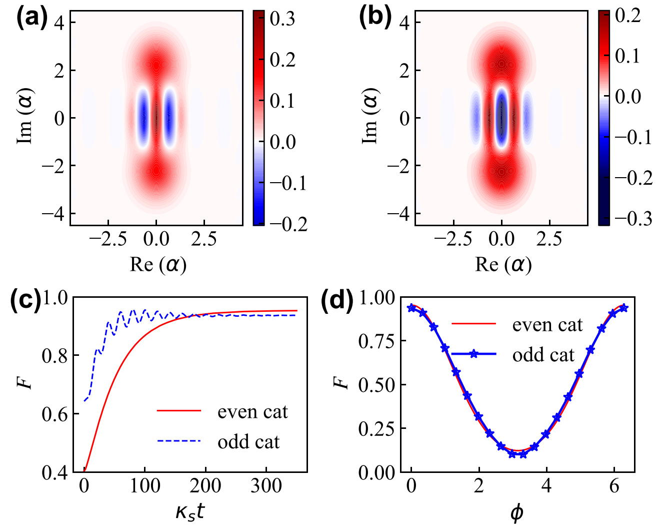

FIG. 2. (a),(b) The Wigner function of the even and odd cat state. (c) The time evolution of fidelity of even (red curve) and odd (blue curve) cat state using the original Hamiltonian. (d) The fidelity of the even cat state and odd cat state versus initial phase ϕ. The parameters are chosen as $\Delta = 10\kappa_s$, $g_1 = \kappa_s$, $g = 2\kappa_s$, $\Omega_s = 0.1\kappa_s$, $\kappa_m = 0$, $|\alpha| = 1.58$, (a),(b),(c) $\phi = 0$.

the ideal Schrödinger cat state and the actual state, i.e., $F = \text{Tr}(\rho_r\rho_0)$, where ρ_0 is the ideal Schrödinger cat state and ρ_r is the actual reduced density matrix of the magnon coming from Eq. (1). From Fig. 2(c), we find that F gradually increases and eventually stabilizes at $F = 0.96$ ($F = 0.94$) for even (odd) cat state after reaching the steady state, showing that the scheme of parametric coupling transfer to produce the magnon cat state is sufficiently effective. It is worth noting that the time evolution of fidelity F exhibits fast oscillation [the blue curve in Fig. 2(c)] when the magnon m is initially in the nonzero Fock state. We speculate the reason is that $g^2/(\Delta)m^\dagger m$ in the second-order Hamiltonian has a strong influence on the system evolution at nonzero Fock states, i.e., $g^2/(\Delta)m^\dagger m|0\rangle = 0$ and $g^2/(\Delta)m^\dagger m|1\rangle = g^2/\Delta|1\rangle$, resulting in the fidelity of the cat state oscillating rapidly.

The initial phase ϕ of the driving field has an effect on the cat-state evolution of the system. We plot the fidelity F versus ϕ by solving the master equation using the original Hamiltonian in Eq. (1), as shown in Fig. 2(d). The magnon state is close to the ideal cat state, i.e., $F = 0.96$ when the initial phase is an even multiple of π, i.e., $\phi = \pm n\pi$, $n \in (0, 2, 4\cdots)$ for both odd and even cat states. However, the fidelity is lowest, i.e., $F = 0.1$ when the initial phase is an odd multiple of π, i.e., $\phi = \pm n\pi$, $n \in (1, 3, 5\cdots)$, implying that the generation of the magnon cat state is phase sensitive. Therefore, in practical experiments, we need to tune the phase of the driving field to an even multiple of π or its vicinity to obtain a high-fidelity magnon cat state. Considering the above facts, in the subsequent

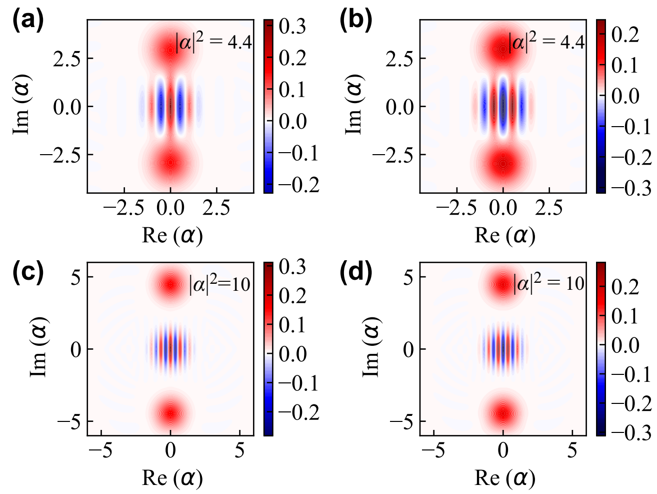

FIG. 3. The Wigner function of magnon even (a),(c) and odd (b),(d) cat state with different sizes. The parameters are chosen as (a),(b) $g_1 = \kappa_s$, $g = 1.5\kappa_s$, $\Omega_s = 0.1\kappa_s$, $|\alpha| = 2.108$, (c),(d) $g_1 = 0.5\kappa_s$, $g = 2\kappa_s$, $\Omega_s = 0.2\kappa_s$, $|\alpha| = 3.3$. Other parameters are the same as in Fig. 2.

sections, we set $\phi = 0$ and do not discuss the effect of the initial phase on the system anymore.

IV. THE SIZE OF MAGNON CAT STATE AND THE SPEED OF ITS GENERATION

The square distance between two coherent states in phase space characterizes the size of the cat states. From the coherent amplitude $\alpha = \sqrt{-\Omega_s\Delta^2/g_1 g^2}$, we can find that the size of the cat state is affected by many degrees of freedom of the system, which means that the size of the magnon cat state can be easily adjusted by changing the parameters in our scheme. In Figs. 3(a) and 3(b), we plot the Wigner function of the magnon cat state with coherent amplitude $|\alpha| = 2.108$ by setting $g = 1.5\kappa_s$ and $g_1 = \kappa_s$. Compared to Figs. 2(a) and 2(b), the two peaks of the superposition state are shifted farther in the phase space and more interference fringes appear, suggesting that a larger size cat state has been generated. It is worth noting that the parametric coupling strength g_1 is more challenging compared to the implementation of the coupling strength g. However, the parametric coupling g_1 can be compensated by the coupling strength g in our scheme. For example, a large size cat state with coherent amplitude $|\alpha| = 2.23$ can also be generated by reducing the parametric coupling strength g_1, i.e., $g_1 = 0.5\kappa_s$ and setting $g = 2\kappa_s$. Due to the negative relationship between g (g_1) and the size of cat state, their contribution to the cat state size is limited. In our scheme, the driving strength Ω_s can effectively increase the size of the magnon cat state. By increasing the driving strength $\Omega_s = 0.2\kappa_s$, the size of the magnon cat state can reach $|\alpha|^2 = 10$ when $g = 2\kappa_s$, $g_1 = 0.5\kappa_s$ and $\Delta = 10\kappa_s$, as shown in Figs. 3(c) and 3(d).

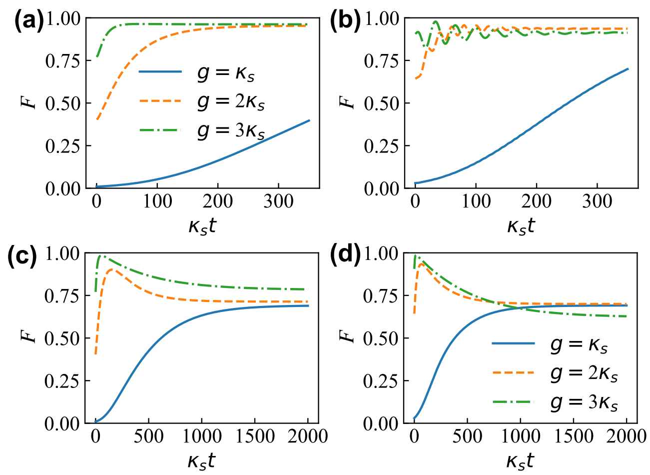

FIG. 4. (a),(b) The fidelity of the even and odd cat state versus $\kappa_s t$ under different coupling strengths. (c),(d) The fidelity of the even and odd cat state versus $\kappa_s t$ with the simultaneous single-magnon dissipation and two-magnon loss under different coupling strengths. The parameters are chosen as $g_1 = \kappa_s$, (a),(b) $\kappa_m = 0$, (c),(d) $\kappa_m = 0.001\kappa_s$. Other parameters are the same as in Fig. 2.

This indicates that the cat state with super-large size has been generated. The above analysis shows that our scheme can easily adjust the size of the cat state, and the large size of the cat state can also be generated.

The speed of cat-state generation is useful in practical applications and is affected by the effective two-magnon loss rate. From Eq. (5) we know that two-magnon loss rate induced by the photon parametric coupling is $\kappa_{\rm eff} = 4g_1^2 g^4/\kappa_s\Delta^4$. It is easy to see that it is proportional to the parametric coupling strength g_1 and the photon-magnon interaction strength g. So the effective two-magnon loss rate $\kappa_{\rm eff}$ can be enhanced by adjusting g and g_1 to make the magnon reach the Schrödinger cat state more quickly [44]. We plot the time evolution of the fidelity F with different photon-magnon interaction strengths in Figs. 4(a) and 4(b) using the original Hamiltonian Eq. (1). It is not difficult to find that the system takes a longer time to reach the cat state when the coupling strength g is smaller. The speed of cat-state generation gradually increases as g increases (seeing the curves in three different colors). In Fig. 4(b), the oscillation of fidelity F becomes more intense as g increases when the magnon m is initially in the nonzero Fock state. This reason is that the offset of the magnon frequency g^2/Δ also increases as g increases. Meanwhile, we notice that the even (odd) cat state with high fidelity $F_{\rm max} = 0.95$ ($F_{\rm max} = 0.97$) can be obtained under strong coupling strength, i.e., $g = 3\kappa_s$, implying that the increase of coupling strength will contribute to the fidelity. We note that the competition between the size and fidelity of the generated cat state limits the choice of coupling strength g. However, in our scheme, the driving strength Ω_s can compensate for the cost of improving the speed

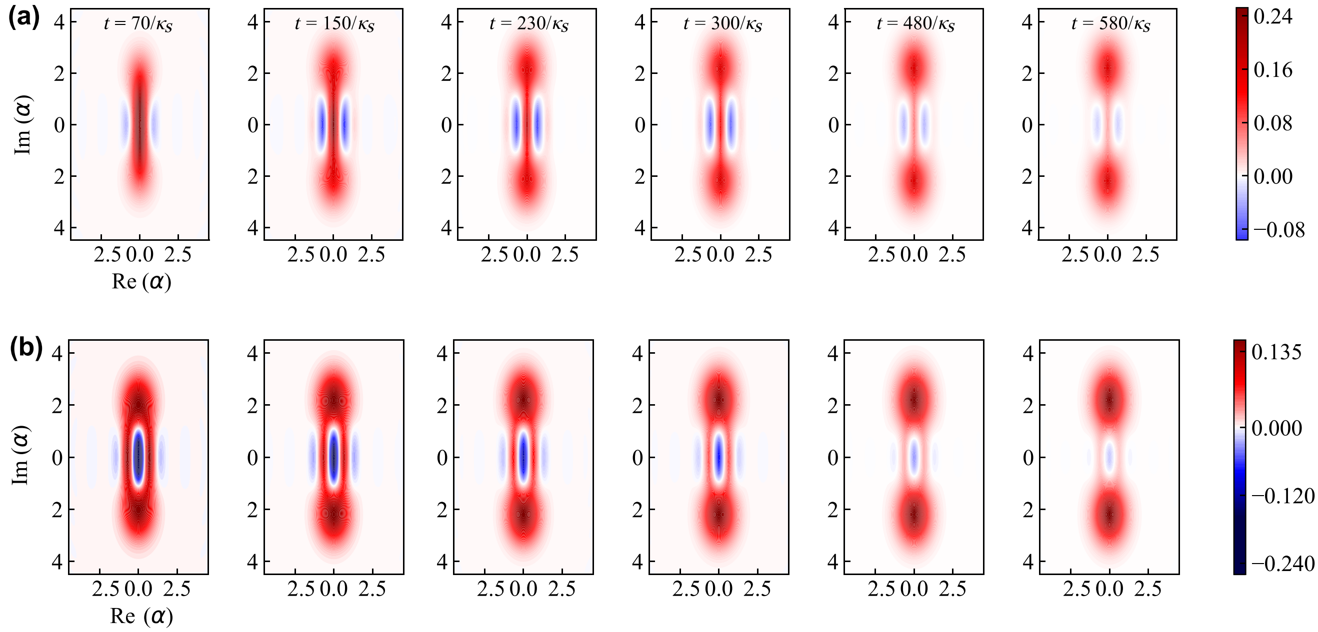

FIG. 5. (a),(b) The Wigner function of the even and odd cat state with the simultaneous single-magnon dissipation and two-magnon loss at different instants. The parameters are chosen as $g_1 = \kappa_s$, $g = 2\kappa_s$, $\Delta = 10\kappa_s$, and $\kappa_m = 0.001\kappa_s$. Other parameters are the same as in Fig. 2.

of cat-state generation to some extent. For example, we can increase driving strength Ω_s from $0.1\kappa_s$ to $0.25\kappa_s$ to maintain the coherent amplitude α unchanged when coupling strength g increases from $2\kappa_s$ to $3\kappa_s$. Therefore, our scheme allows us to select the stronger coupling strength g to improve the speed of cat-state generation with high fidelity and ensure the size of cat state in the actual cat-state preparation.

V. INFLUENCE OF SINGLE-MAGNON DISSIPATION

Single-magnon dissipation κ_m is inevitable in real physical systems, which is the main factor limiting the size and lifetime of magnon cat state. In this section we will analyze the dynamical evolution of the magnon under considering the single-magnon dissipation κ_m. The master equation including single-magnon dissipation is written as

$$\dot{\rho_m} = -i[H_{\text{eff}}, \rho] + (\kappa_{\text{eff}}/2)\mathcal{L}[m^2]\rho_m + (\kappa_m/2)\mathcal{L}[m]\rho_m, \qquad (9)$$

where $\mathcal{L}[m]\rho = 2m\rho m^\dagger - m^\dagger m\rho - \rho m^\dagger m$ is the single-magnon dissipation term. As shown in Figs. 4(c) and 4(d) (the orange curve), we plot the time evolution of the fidelity $F(\text{Tr}(\rho_m\rho_0))$ of the magnon density matrix ρ_m under the parameter $g = 2\kappa_s$ using the effective Hamiltonian. The fidelity F of the even (odd) magnon cat state reaches its maximum $F = 0.9$ ($F = 0.93$) at $t \sim 150/\kappa_s$ ($t \sim 70/\kappa_s$), and then decreases gradually until it stabilizes at $F = 0.7$. This shows that the single-magnon dissipation greatly destroys the generation of cat states, and steers the magnon to evolve to a mixture of two coherent states. This can also be confirmed by the Wigner function of the magnon density matrix ρ_m as shown in Fig. 5. At $t \sim 150/\kappa_s$ ($t \sim 70/\kappa_s$), the distance between the two peaks of the coherent state reaches the maximum, and the interference fringes are also the most obvious, meaning that the magnon enters the cat-state manifold. However, at $t \sim 480/\kappa_s$, the interference fringes gradually disappear and magnon finally evolves into a mixture of two coherent states, implying that the coherence is destroyed under the influence of single-magnon dissipation. The results above show that the single-magnon dissipation is detrimental to the production of the magnon cat state.

Next, let us study the effect of single-magnon dissipation on the speed of the cat state generation. We have known that the strong coupling strength g can rapidly bring the magnon to the cat state with high fidelity without considering the single-magnon dissipation. Likewise, similar conclusion is still established under the influence of single-magnon dissipation. The time evolution of the fidelity F is plotted in Figs. 4(c) and 4(d) using Eq. (9). From the figure we find that the stronger coupling strength g, the faster speed of the even (odd) cat-state generation. For example, when $g = 3\kappa_s$, the fidelity F undergoes a sharp rise to reach the maximum $F = 0.98$ ($F = 0.98$) at $t = 50/\kappa_s$ ($t = 15/\kappa_s$). This shows that the cat state with high fidelity is rapidly prepared. It is worth noting that the speed of the odd cat-state generation is much faster than that of the even

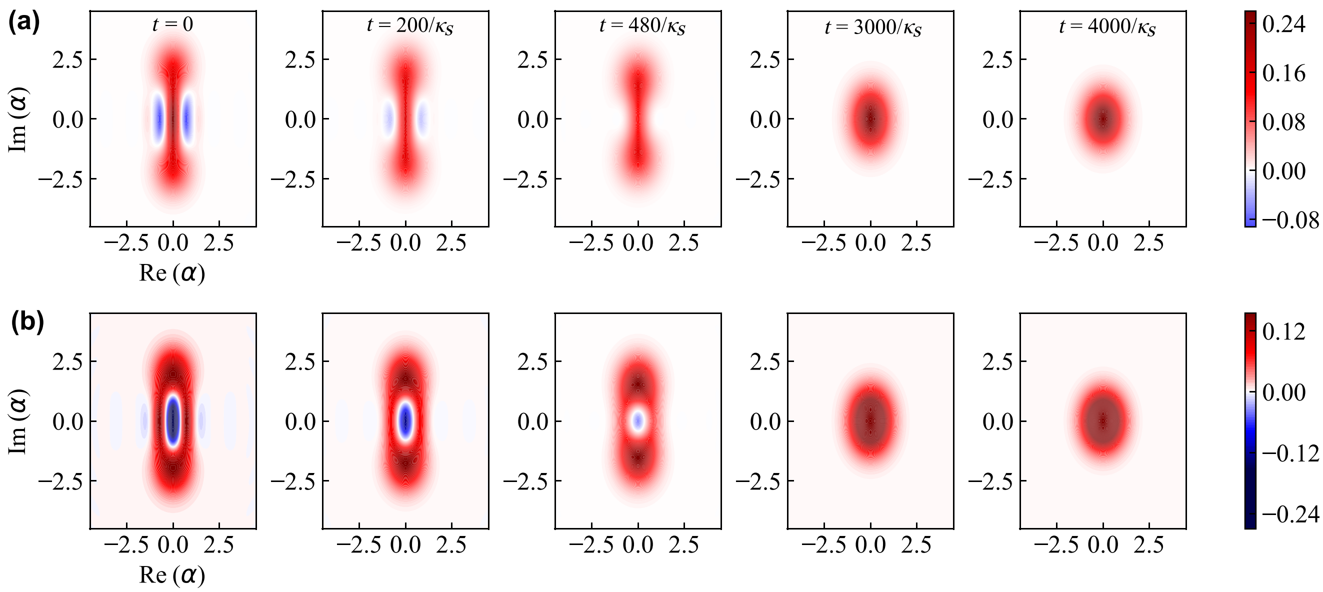

FIG. 6. (a),(b) The Wigner function of the even and odd cat state with only the single-magnon dissipation at different instants. The parameters are chosen as $g_1 = \kappa_s$, $g = 2\kappa_s$, $\Delta = 10\kappa_s$, and $\kappa_m = 0.001\kappa_s$. Other parameters are the same as in Fig. 2.

cat state under the same parameter conditions. Therefore, the odd cat state can be a good choice in applications that require rapid preparation of cat states. However, the cost of speedup is the rapid decline on fidelity. For example, the fidelity of the odd cat state $F = 0.75$ at $t = 500/\kappa_s$ when $g = 3\kappa_s$, far less than the fidelity $F = 0.85$ of the even cat state at $t = 500/\kappa_s$. These results indicate that the single-magnon dissipation has different effects on the even and odd cat states. Meanwhile, we also note that when the coupling strength is small, i.e., $g = \kappa_s$, the fidelity of the system is low as shown in the blue curve in Figs. 4(c) and 4(d), implying that the magnon mode m does not evolve to the cat state. The reason is as follows. The generation of the magnon cat state depends essentially on the effective two-magnon loss rate $\kappa_{\rm eff}$. When $\kappa_{\rm eff} \gg \kappa_m$, the two-magnon loss can strongly suppress the single-magnon dissipation, steering the magnon into the cat state manifold. When $\kappa_{\rm eff} \ll \kappa_m$, the effective two-magnon loss process is suppressed by the single-magnon dissipation, making the cat-state manifold be destroyed and the cat state be not generated. Specifically, the single-magnon dissipation rate $\kappa_m = 0.001\kappa_s$ is much larger than the effective two-magnon loss rate $\kappa_{\rm eff} = 0.0004\kappa_s$ when the coupling strength g is small, i.e., $g = \kappa_s$, which leads to a severe suppression of the two-magnon loss process and destroys the generation of the cat states, i.e., $F_{\rm max} = 0.7$. Therefore, synthesizing the above discussion, in order to obtain magnon cat states more quickly with high fidelity, we need to choose suitable parameters to enhance the effective two-magnon loss rate.

We are also interested in the lifetime of the magnon cat state. After the magnon evolved to the cat state with high fidelity, the two-photon loss channel is turned off (setting $g = 0$ so that the magnon does not interact with the cavity). At this time the magnon m is only subjected to single-magnon dissipation. The coherence of the magnon superposition state and the energy of the magnon disappear under the effect of single-magnon dissipation. In order to see more clearly, we plot the Wigner function of the magnon as shown in Fig. 6. The initial two peaks and interference fringes gradually disappear and the magnon finally stabilizes in the vacuum state. Meanwhile, the time evolution of fidelity F is also plotted in Fig. 7. We can see that the fidelity of the even (odd) cat state is negatively correlated with $\kappa_s t$, implying the decay of the coherence and energy of magnon. In Fig. 7(a), the fidelity of the cat state $F = 0.77$ is relatively higher in the steady state due to the smaller coherence amplitude $\alpha \sim 1.1$ when the coupling strength is $g = 3\kappa_s$. Meanwhile, the smaller coherence amplitude, i.e., $\alpha \sim 1.1$, also brings its advantages, such as prolonging the lifetime of the cat state (seeing the blue curve in Fig. 7). We note that there is a large difference on fidelity between the even and odd cat states in the steady state, i.e., $F \sim 0.4$ ($F \sim 0.75$) in Fig. 7(a) and $F \sim 0$ in Fig. 7(b) when $g = 2\kappa_s$ ($g = 3\kappa_s$). The reason is that the ideal even cat state is more similar to the vacuum state when the size of the cat state is not large. The lifetime of the cat state is evaluated by $\tau = 1/2|\alpha|^2\kappa_m$ [96], which is inversely proportional to the magnitude of the coherence amplitude α and the single-magnon dissipation κ_m. When the coherent amplitude $|\alpha| > 1$, the two coherent states are approximately distinguishable [34]. So when $|\alpha| > 1$ is guaranteed, the single-magnon dissipation rate must be reduced as much as possible in order to prolong the lifetime

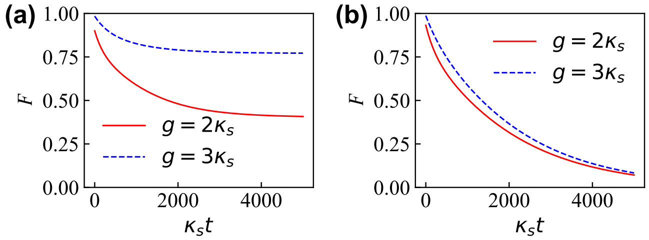

FIG. 7. (a),(b) The fidelity of the even and odd cat state versus $\kappa_s t$ with only the single-magnon dissipation. The parameters are chosen as $g_1 = \kappa_s$, $\Delta = 10\kappa_s$, and $\kappa_m = 0.001\kappa_s$. Other parameters are the same as in Fig. 2.

of the magnon cat state. Due to the low dissipation rate of the magnon, one can expect a lifetime gain. For a modest decay rate of the magnon mode $\kappa_m \sim 1$ MHz, the lifetime of the state will be the order of microsecond. Under the state-of-the-art experimental conditions, the magnon linewidth of $\kappa_m \sim 0.1$ MHz is promising to be realized. When the size of cat state $|\alpha|^2 \sim 1.58$, the lifetime of cat state can reach approximately 3 μs.

VI. DISCUSSION AND CONCLUSION

The cat state not only plays a role in the discussion of the classical and quantum boundary, but also is an indispensable resource for many applications. For example, the cat state can be used to emulate Schrödinger's thought experiment and characterize quantum decoherence in the open system [15]. Also, the cat state, as a nonclassical resource with Wigner negativity, has been proposed to enhance the fidelity of continuous-variable teleportation and implement a loophole-free Bell test [27]. Finally, the cat state can also be used to encode deterministically quantum information, which could enable applications in metrology and quantum information processing [30].

A range of different approaches can be used for experimental setup of our scheme. On the one hand, the superconducting quantum circuits [97] provide a feasible experimental scheme. The pump cavity and the signal cavity can be obtained by the LC oscillators. The parametric coupling between the two cavities can be induced by the Josephson junction with coupling energy E_J and capacitance C_J [92,93]. Experimentally, the magnons can couple with the coplanar waveguide cavity (CPW) and reach the strong coupling regime [98,99]. Therefore, our proposed scheme can be implemented by coupling the CPW with a YIG sphere (placing on top of a CPW or levitation [100]) to a LC oscillator through Josephson junction. On the other hand, the pump cavity and the signal cavity can also be obtained by using two three-dimensional (3D) cavities, and the parametric coupling between them can be realized by the Josephson junction [91,92]. The coherent coupling magnon-photon scheme has been reported experimentally [68]. Thus, by placing a YIG sphere in the signal cavity, the other feasible experimental setup of our scheme can also be established.

Meanwhile, the parameters we selected are feasible under the current experimental conditions. The size, lifetime, and fidelity of the magnon cat state are affected by the photon-magnon interaction strength. The photon-magnon interaction strength with $g > 20$ MHz has been experimentally reported [98,99]. Benefiting from the small microcavity volume and the large YIG sphere volume, g can reach approximately GHz and enter the ultrastrong coupling regime [68]. The parametric coupling strength can reach $g_1 = 50$ MHz (we choose $g_1 = \kappa_s \sim 20$ MHz). Furthermore, using the RWA is effective in the $g < 8\kappa$ regime (e.g., to discard the nonresonant term in the initial Hamiltonian) and has been experimentally confirmed [79].

In summary, we propose an alternative scheme to generate the magnon cat state. The effective two-magnon loss process can be induced by the photon parametric coupling, and then the magnon mode enters the cat-state manifold. The size of generated cat state can be easily adjusted, and we can produce large size cat state with high fidelity. At the same time, the photon-magnon interaction strength directly affects the speed of the cat state generation. The stronger photon-magnon coupling strength, the faster speed of the cat-state generation. We also investigate the influence of environmental decoherence on cat-state preparation and find that the two-magnon loss process induced by photon parametric coupling can strongly suppress the decoherence of the environment when the two-magnon loss is much larger than the single-magnon dissipation. Further, we analyze the lifetime of cat states, which is expected to be $t \sim 3$ μs under the state-of-the-art experimental techniques. Meanwhile, our scheme does not require the direct magnon nonlinearity, which to some extent improves the feasibility of experimental preparation of magnon cat state and provides a solution for the generation of the cat state. It is meaningful for the preparation of fragile quantum states and provides a theoretical solution for observing macroscopic quantum coherence.

ACKNOWLEDGMENTS

We thank Dr. Chang-Sheng Hu, Zi-Hao Li, and Wen Huang for technical support and helpful discussions. This work was supported by the National Key Research and Development Program of China (Grant No. 2021YFA1400702); National Natural Science Foundation of China (Grant No. 11975103).

APPENDIX: DERIVATION OF STEADY MAGNON CAT STATE

An effective master equation [Eq. (5)] is

$$\dot{\rho} = -i[H_{\text{eff}}, \rho] + (\kappa_{\text{eff}}/2)\mathcal{L}[m^2]\rho. \tag{A1}$$

By setting $\dot{\rho} = 0$, we can obtain

$$-i[H_{\text{eff}}, \rho] + (\kappa_{\text{eff}}/2)\mathcal{L}[m^2] = 0. \tag{A2}$$

Substituting the effective Hamiltonian H_{eff} and the two-magnon loss κ_{eff}, the steady-state equation can be written as

$$\hat{D}|\psi\rangle\langle\psi|m^{\dagger 2} - m^{\dagger 2}\hat{D}|\psi\rangle\langle\psi| + \text{H.c} = 0, \tag{A3}$$

where $\hat{D} = (\kappa_{\text{eff}}/(2)m^2 - iJ)$ and we have set $\rho = |\psi\rangle\langle\psi|$ and $\phi = 0$. This indicates that the steady state $|\psi\rangle$ satisfies

$$\left(\frac{\kappa_{\text{eff}}}{2}m^2 - iJ\right)|\psi\rangle = 0. \tag{A4}$$

Because $\alpha^2 = i2J/\kappa_{\text{eff}}$, we can rewrite the equation as

$$(m^2 - \alpha^2)|\psi\rangle = 0. \tag{A5}$$

We express $|\psi\rangle$, in terms of the Fock-state $|n\rangle$, as

$$|\psi\rangle = \sum_n c_n|n\rangle.$$

Here, n refers to the number of excited magnons in the YIG sphere and c_n is the probability amplitude. The condition in Eq. (A5) gives a recursion relation as follows:

$$c_{n+2}\sqrt{n+2}\sqrt{n+1} = \alpha^2 c_n, \tag{A6}$$

where $n \geq 0$. The recursion relation in Eq. (A6) reveals that, when the magnon is initially in a Fock state $|n\rangle$ with an even n, i.e., in the ground state $|0\rangle$, the steady state $|\psi\rangle$ can be expressed as

$$|\psi\rangle = \sqrt{\frac{2}{e^{|\alpha|^2} + e^{-|\alpha|^2}}} \sum_{n=\text{even}} \frac{\alpha^n}{\sqrt{n!}}|n\rangle. \tag{A7}$$

Similarly, when the magnon is initially in the Fock state $|n\rangle$ with an odd n, i.e., in the single-excitation state $|1\rangle$, the steady state $|\psi\rangle$ becomes

$$|\psi\rangle = \sqrt{\frac{2}{e^{|\alpha|^2} - e^{-|\alpha|^2}}} \sum_{n=\text{odd}} \frac{\alpha^n}{\sqrt{n!}}|n\rangle. \tag{A8}$$

From Eqs. (A7) and (A8), it is not difficult to find that they are the expressions of cat states.

[1] Erwin Schrödinger, Die gegenwärtige situation in der quantenmechanik, Naturwissenschaften **23**, 844 (1935).

[2] Yunjie Xia and Guangcan Guo, Nonclassical properties of even and odd coherent states, Phys. Lett. A **136**, 281 (1989).

[3] J. Janszky and A. V. Vinogradov, Squeezing via one-dimensional distribution of coherent states, Phys. Rev. Lett. **64**, 2771 (1990).

[4] J. Janszky, P. Domokos, and P. Adam, Coherent states on a circle and quantum interference, Phys. Rev. A **48**, 2213 (1993).

[5] J. Janszky, P. Domokos, S. Szabó, and P. Adam, Quantum-state engineering via discrete coherent-state superpositions, Phys. Rev. A **51**, 4191 (1995).

[6] Marlan O. Scully and M. Suhail Zubairy, *Quantum Optics* (Cambridge University Press, Cambridge, 1997).

[7] Barry C. Sanders, Review of entangled coherent states, J. Phys. A: Math. Theor. **45**, 244002 (2012).

[8] Barry C. Sanders, Entangled coherent states, Phys. Rev. A **45**, 6811 (1992).

[9] Jérôme Wenger, Mohammad Hafezi, Frédéric Grosshans, Rosa Tualle-Brouri, and Philippe Grangier, Maximal violation of Bell inequalities using continuous-variable measurements, Phys. Rev. A **67**, 012105 (2003).

[10] H. Jeong, W. Son, M. S. Kim, D. Ahn, and Č. Brukner, Quantum nonlocality test for continuous-variable states with dichotomic observables, Phys. Rev. A **67**, 012106 (2003).

[11] Wojciech Hubert Zurek, Decoherence, einselection, and the quantum origins of the classical, Rev. Mod. Phys. **75**, 715 (2003).

[12] Magdalena Stobińska, Hyunseok Jeong, and Timothy C. Ralph, Violation of Bell's inequality using classical measurements and nonlinear local operations, Phys. Rev. A **75**, 052105 (2007).

[13] Serge Haroche, Nobel lecture: Controlling photons in a box and exploring the quantum to classical boundary, Rev. Mod. Phys. **85**, 1083 (2013).

[14] M. Brune, E. Hagley, J. Dreyer, X. Maître, A. Maali, C. Wunderlich, J. M. Raimond, and S. Haroche, Observing the progressive decoherence of the "meter" in a quantum measurement, Phys. Rev. Lett. **77**, 4887 (1996).

[15] C. Monroe, D. M. Meekhof, B. E. King, and D. J. Wineland, A "Schrödinger cat" superposition state of an atom, Science **272**, 1131 (1996).

[16] T. C. Ralph, A. Gilchrist, G. J. Milburn, W. J. Munro, and S. Glancy, Quantum computation with optical coherent states, Phys. Rev. A **68**, 042319 (2003).

[17] A. Gilchrist, Kae Nemoto, W. J. Munro, T. C. Ralph, S Glancy, Samuel L. Braunstein, and G. J. Milburn, Schrödinger cats and their power for quantum information processing, J. Opt. B: Quantum Semiclass. Opt. **6**, S828 (2004).

[18] Mile Gu, Computing with quantum cats: From colossus to qubits, Phys. Today **68**, 46 (2015).

[19] Weizhou Cai, Yuwei Ma, Weiting Wang, Chang-Ling Zou, and Luyan Sun, Bosonic quantum error correction codes in superconducting quantum circuits, Fund. Res **1**, 50 (2021).

[20] Mackillo Kira, Stephan W. Koch, Ryan P. Smith, Andrew E. Hunter, and Steven T. Cundiff, Quantum spectroscopy with Schrödinger-cat states, Nat. Phys. **7**, 799 (2011).

[21] Luca Pezzè, Augusto Smerzi, Markus K. Oberthaler, Roman Schmied, and Philipp Treutlein, Quantum metrology with nonclassical states of atomic ensembles, Rev. Mod. Phys. **90**, 035005 (2018).
[22] G. S. Agarwal, R. R. Puri, and R. P. Singh, Atomic Schrödinger cat states, Phys. Rev. A **56**, 2249 (1997).
[23] S. Mancini, V. I. Man'ko, and P. Tombesi, Ponderomotive control of quantum macroscopic coherence, Phys. Rev. A **55**, 3042 (1997).
[24] S. Bose, K. Jacobs, and P. L. Knight, Preparation of nonclassical states in cavities with a moving mirror, Phys. Rev. A **56**, 4175 (1997).
[25] Cass A. Sackett, David Kielpinski, Brian E. King, Christopher Langer, Volker Meyer, Christopher J. Myatt, M. Rowe, Q. A. Turchette, Wayne M. Itano, David J. Wineland, and C. Monroe, Experimental entanglement of four particles, Nature **404**, 256 (2000).
[26] Dietrich Leibfried, Emanuel Knill, Signe Seidelin, Joe Britton, R. Brad Blakestad, John Chiaverini, David B. Hume, Wayne M. Itano, John D. Jost, Christopher Langer, R. Ozeri, R. Reichle, and D. J. Wineland, Creation of a six-atom "Schrödinger cat" state, Nature **438**, 639 (2005).
[27] Alexei Ourjoumtsev, Rosa Tualle-Brouri, Julien Laurat, and Philippe Grangier, Generating optical Schrödinger kittens for quantum information processing, Science **312**, 83 (2006).
[28] Alexei Ourjoumtsev, Hyunseok Jeong, Rosa Tualle-Brouri, and Philippe Grangier, Generation of optical "Schrödinger cats" from photon number states, Nature **448**, 784 (2007).
[29] Thomas Monz, Philipp Schindler, Julio T. Barreiro, Michael Chwalla, Daniel Nigg, William A. Coish, Maximilian Harlander, Wolfgang Hänsel, Markus Hennrich, and Rainer Blatt, 14-qubit entanglement: Creation and coherence, Phys. Rev. Lett. **106**, 130506 (2011).
[30] Brian Vlastakis, Gerhard Kirchmair, Zaki Leghtas, Simon E. Nigg, Luigi Frunzio, S. M. Girvin, Mazyar Mirrahimi, M. H. Devoret, and R. J. Schoelkopf, Deterministically encoding quantum information using 100-photon Schrödinger cat states, Science **342**, 607 (2013).
[31] Hon Wai Lau, Zachary Dutton, Tian Wang, and Christoph Simon, Proposal for the creation and optical detection of spin cat states in Bose-Einstein condensates, Phys. Rev. Lett. **113**, 090401 (2014).
[32] Mark J. Everitt, Timothy P. Spiller, Gerard J. Milburn, Richard D. Wilson, and Alexandre M. Zagoskin, Engineering dissipative channels for realizing Schrödinger cats in squids, Front. ICT **1**, 1 (2014).
[33] Jean Etesse, Martin Bouillard, Bhaskar Kanseri, and Rosa Tualle-Brouri, Experimental generation of squeezed cat states with an operation allowing iterative growth, Phys. Rev. Lett. **114**, 193602 (2015).
[34] Jie-Qiao Liao and Lin Tian, Macroscopic quantum superposition in cavity optomechanics, Phys. Rev. Lett. **116**, 163602 (2016).
[35] Jie-Qiao Liao, Jin-Feng Huang, and Lin Tian, Generation of macroscopic Schrödinger-cat states in qubit-oscillator systems, Phys. Rev. A **93**, 033853 (2016).
[36] C. E. Bradley, J. Randall, M. H. Abobeih, R. C. Berrevoets, M. J. Degen, M. A. Bakker, M. Markham, D. J. Twitchen, and T. H. Taminiau, A ten-qubit solid-state spin register with quantum memory up to one minute, Phys. Rev. X **9**, 031045 (2019).
[37] Yao Lu, Shuaining Zhang, Kuan Zhang, Wentao Chen, Yangchao Shen, Jialiang Zhang, Jing-Ning Zhang, and Kihwan Kim, Global entangling gates on arbitrary ion qubits, Nature **572**, 363 (2019).
[38] Caroline Figgatt, Aaron Ostrander, Norbert M. Linke, Kevin A. Landsman, Daiwei Zhu, Dmitri Maslov, and Christopher Monroe, Parallel entangling operations on a universal ion-trap quantum computer, Nature **572**, 368 (2019).
[39] A. Omran, H. Levine, A. Keesling, G. Semeghini, T. T. Wang, S. Ebadi, H. Bernien, A. S. Zibrov, H. Pichler, S. Choi, J. Cui, M. Rossignolo, P. Rembold, S. Montangero, T. Calarco, M. Endres, M. Greiner, V. Vuletić, and M. D. Lukin, Generation and manipulation of Schrödinger cat states in Rydberg atom arrays, Science **365**, 570 (2019).
[40] Chao Song, Kai Xu, Hekang Li, Yu-Ran Zhang, Xu Zhang, Wuxin Liu, Qiujiang Guo, Zhen Wang, Wenhui Ren, Jie Hao, Hui Feng, Heng Fan, Dongning Zheng, Da-Wei Wang, H. Wang, and Shi-Yao Zhu, Generation of multicomponent atomic Schrödinger cat states of up to 20 qubits, Science **365**, 574 (2019).
[41] Ken X. Wei, Isaac Lauer, Srikanth Srinivasan, Neereja Sundaresan, Douglas T. McClure, David Toyli, David C. McKay, Jay M. Gambetta, and Sarah Sheldon, Verifying multipartite entangled Greenberger-Horne-Zeilinger states via multiple quantum coherences, Phys. Rev. A **101**, 032343 (2020).
[42] Ye-Hong Chen, Wei Qin, Xin Wang, Adam Miranowicz, and Franco Nori, Shortcuts to adiabaticity for the quantum Rabi model: Efficient generation of giant entangled cat states via parametric amplification, Phys. Rev. Lett. **126**, 023602 (2021).
[43] Wei Qin, Adam Miranowicz, Hui Jing, and Franco Nori, Generating long-lived macroscopically distinct superposition states in atomic ensembles, Phys. Rev. Lett. **127**, 093602 (2021).
[44] Zhucheng Zhang, Lei Shao, Wangjun Lu, and Xiaoguang Wang, All-optical generation of deterministic squeezed Schrödinger-cat states, Phys. Rev. A **106**, 043721 (2022).
[45] Christopher C. Gerry and Edwin E. Hach, Generation of even and odd coherent states in a competitive two-photon process, Phys. Lett. A **174**, 185 (1993).
[46] L. Gilles, B. M. Garraway, and P. L. Knight, Generation of nonclassical light by dissipative two-photon processes, Phys. Rev. A **49**, 2785 (1994).
[47] Markus Arndt and Klaus Hornberger, Testing the limits of quantum mechanical superpositions, Nat. Phys. **10**, 271 (2014).
[48] John Clarke, Andrew N. Cleland, Michel H. Devoret, Daniel Esteve, and John M. Martinis, Quantum mechanics of a macroscopic variable: The phase difference of a Josephson junction, Science **239**, 992 (1988).
[49] Jonathan R. Friedman, Vijay Patel, Wei Chen, S. K. Tolpygo, and James E. Lukens, Quantum superposition of distinct macroscopic states, Nature **406**, 43 (2000).
[50] Caspar H. van der Wal, A. C. J. ter Haar, F. K. Wilhelm, R. N. Schouten, C. J. P. M. Harmans, T. P. Orlando,

Seth Lloyd, and J. E. Mooij, Quantum superposition of macroscopic persistent-current states, Science **290**, 773 (2000).

[51] J. S. Neergaard-Nielsen, B. Melholt Nielsen, C. Hettich, K. Mølmer, and E. S. Polzik, Generation of a superposition of odd photon number states for quantum information networks, Phys. Rev. Lett. **97**, 083604 (2006).

[52] Markus Arndt, Olaf Nairz, Julian Vos-Andreae, Claudia Keller, Gerbrand Van der Zouw, and Anton Zeilinger, Wave–particle duality of C_{60} molecules, Nature **401**, 680 (1999).

[53] Ze-Liang Xiang, Sahel Ashhab, J. Q. You, and Franco Nori, Hybrid quantum circuits: Superconducting circuits interacting with other quantum systems, Rev. Mod. Phys. **85**, 623 (2013).

[54] Guo-Qiang Zhang, Zhen Chen, Da Xu, Nathan Shammah, Meiyong Liao, Tie-Fu Li, Limin Tong, Shi-Yao Zhu, Franco Nori, and J. Q. You, Exceptional point and cross-relaxation effect in a hybrid quantum system, PRX Quantum **2**, 020307 (2021).

[55] Hans Huebl, Christoph W. Zollitsch, Johannes Lotze, Fredrik Hocke, Moritz Greifenstein, Achim Marx, Rudolf Gross, and Sebastian T. B. Goennenwein, High cooperativity in coupled microwave resonator ferrimagnetic insulator hybrids, Phys. Rev. Lett. **111**, 127003 (2013).

[56] Lihui Bai, M. Harder, Y. P. Chen, X. Fan, J. Q. Xiao, and C.-M. Hu, Spin pumping in electrodynamically coupled magnon-photon systems, Phys. Rev. Lett. **114**, 227201 (2015).

[57] Dengke Zhang, Xin-Ming Wang, Tie-Fu Li, Xiao-Qing Luo, Weidong Wu, Franco Nori, and J. Q. You, Cavity quantum electrodynamics with ferromagnetic magnons in a small yttrium-iron-garnet sphere, Npj Quantum Inf. **1**, 1 (2015).

[58] Dengke Zhang, Xiao-Qing Luo, Yi-Pu Wang, Tie-Fu Li, and JQ You, Observation of the exceptional point in cavity magnon-polaritons, Nat. Commun. **8**, 1368 (2017).

[59] Yi-Pu Wang, J. W. Rao, Y. Yang, Peng-Chao Xu, Y. S. Gui, B. M. Yao, J. Q. You, and C.-M. Hu, Nonreciprocity and unidirectional invisibility in cavity magnonics, Phys. Rev. Lett. **123**, 127202 (2019).

[60] Ö. O. Soykal and M. E. Flatté, Strong field interactions between a nanomagnet and a photonic cavity, Phys. Rev. Lett. **104**, 077202 (2010).

[61] Wei-Jiang Wu, Yi-Pu Wang, Jin-Ze Wu, and Jie Li, and J. Q. You, Remote magnon entanglement between two massive ferrimagnetic spheres via cavity optomagnonics, Phys. Rev. A **104**, 023711 (2021).

[62] Zhi-Bo Yang, Wei-Jiang Wu, Jie Li, Yi-Pu Wang, and J. Q. You, Steady-entangled-state generation via the cross-Kerr effect in a ferrimagnetic crystal, Phys. Rev. A **106**, 012419 (2022).

[63] Chengsong Zhao, Zhen Yang, Rui Peng, Junya Yang, Chong Li, and Ling Zhou, Dissipative-coupling-induced transparency and high-order sidebands with Kerr nonlinearity in a cavity-magnonics system, Phys. Rev. Appl. **18**, 044074 (2022).

[64] Da-Wei Wang, Chengsong Zhao, Junya Yang, Ye-Ting Yan, and Ling Zhou, Simulating the extended Su-Schrieffer-Heeger model and transferring an entangled state based on a hybrid cavity-magnon array, Phys. Rev. A **107**, 053701 (2023).

[65] Ken-ichi Uchida, J. Xiao, Hiroto Adachi, Jun-ichiro Ohe, Saburo Takahashi, J. Ieda, T. Ota, Y. Kajiwara, H. Umezawa, H. Kawai, G. E. W Bauer, S. Maekawa, and E. Saitoh, Spin Seebeck insulator, Nat. Mater. **9**, 894 (2010).

[66] Y. Kajiwara, K. Harii, S. Takahashi, Jun-ichiro Ohe, K. Uchida, M. Mizuguchi, H. Umezawa, H. Kawai, Kazuya Ando, K. Takanashi, S. Maekawa, and E. Saitoh, Transmission of electrical signals by spin-wave interconversion in a magnetic insulator, Nature **464**, 262 (2010).

[67] Maxim Goryachev, Warrick G. Farr, Daniel L. Creedon, Yaohui Fan, Mikhail Kostylev, and Michael E. Tobar, High-cooperativity cavity QED with magnons at microwave frequencies, Phys. Rev. Appl. **2**, 054002 (2014).

[68] Xufeng Zhang, Chang-Ling Zou, Liang Jiang, and Hong X. Tang, Strongly coupled magnons and cavity microwave photons, Phys. Rev. Lett. **113**, 156401 (2014).

[69] Yutaka Tabuchi, Seiichiro Ishino, Toyofumi Ishikawa, Rekishu Yamazaki, Koji Usami, and Yasunobu Nakamura, Hybridizing ferromagnetic magnons and microwave photons in the quantum limit, Phys. Rev. Lett. **113**, 083603 (2014).

[70] R. Hisatomi, A. Osada, Y. Tabuchi, T. Ishikawa, A. Noguchi, R. Yamazaki, K. Usami, and Y. Nakamura, Bidirectional conversion between microwave and light via ferromagnetic magnons, Phys. Rev. B **93**, 174427 (2016).

[71] A. Osada, R. Hisatomi, A. Noguchi, Y. Tabuchi, R. Yamazaki, K. Usami, M. Sadgrove, R. Yalla, M. Nomura, and Y. Nakamura, Cavity optomagnonics with spin-orbit coupled photons, Phys. Rev. Lett. **116**, 223601 (2016).

[72] Xufeng Zhang, Na Zhu, Chang-Ling Zou, and Hong X. Tang, Optomagnonic whispering gallery microresonators, Phys. Rev. Lett. **117**, 123605 (2016).

[73] A. Osada, A. Gloppe, R. Hisatomi, A. Noguchi, R. Yamazaki, M. Nomura, Y. Nakamura, and K. Usami, Brillouin light scattering by magnetic quasivortices in cavity optomagnonics, Phys. Rev. Lett. **120**, 133602 (2018).

[74] Jie Li, Shi-Yao Zhu, and G. S. Agarwal, Magnon-photon-phonon entanglement in cavity magnomechanics, Phys. Rev. Lett. **121**, 203601 (2018).

[75] Yi-Pu Wang, Guo-Qiang Zhang, Dengke Zhang, Tie-Fu Li, C.-M. Hu, and J. Q. You, Bistability of cavity magnon polaritons, Phys. Rev. Lett. **120**, 057202 (2018).

[76] Yi Li, Tomas Polakovic, Yong-Lei Wang, Jing Xu, Sergi Lendinez, Zhizhi Zhang, Junjia Ding, Trupti Khaire, Hilal Saglam, Ralu Divan, John Pearson, Wai-Kwong Kwok, Zhili Xiao, Valentine Novosad, Axel Hoffmann, and Wei Zhang, Strong coupling between magnons and microwave photons in on-chip ferromagnet-superconductor thin-film devices, Phys. Rev. Lett. **123**, 107701 (2019).

[77] Feng-Yang Zhang, Qi-Cheng Wu, and Chui-Ping Yang, Non-hermitian shortcut to adiabaticity in Floquet cavity electromagnonics, Phys. Rev. A **106**, 012609 (2022).

[78] Rui-Chang Shen, Jie Li, Zhi-Yuan Fan, Yi-Pu Wang, and J. Q. You, Mechanical bistability in Kerr-modified cavity magnomechanics, Phys. Rev. Lett. **129**, 123601 (2022).

[79] Yutaka Tabuchi, Seiichiro Ishino, Atsushi Noguchi, Toyofumi Ishikawa, Rekishu Yamazaki, Koji Usami, and

Yasunobu Nakamura, Coherent coupling between a ferromagnetic magnon and a superconducting qubit, Science **349**, 405 (2015).

[80] Marios Kounalakis, Gerrit E. W. Bauer, and Yaroslav M. Blanter, Analog quantum control of magnonic cat states on a chip by a superconducting qubit, Phys. Rev. Lett. **129**, 037205 (2022).

[81] Zeng-Xing Liu and Hao Xiong, Magnon laser based on Brillouin light scattering, Opt. Lett. **45**, 5452 (2020).

[82] Ye-Jun Xu and Jun Song, Nonreciprocal magnon laser, Opt. Lett. **46**, 5276 (2021).

[83] Kai-Wei Huang, Ying Wu, and Liu-Gang Si, Parametric-amplification-induced nonreciprocal magnon laser, Opt. Lett. **47**, 3311 (2022).

[84] Zeng-Xing Liu, Hao Xiong, and Ying Wu, Magnon blockade in a hybrid ferromagnet-superconductor quantum system, Phys. Rev. B **100**, 134421 (2019).

[85] Akashdeep Kamra and Wolfgang Belzig, Super-poissonian shot noise of squeezed-magnon mediated spin transport, Phys. Rev. Lett. **116**, 146601 (2016).

[86] Akashdeep Kamra and Wolfgang Belzig, Magnon-mediated spin current noise in ferromagnet | nonmagnetic conductor hybrids, Phys. Rev. B **94**, 014419 (2016).

[87] Akashdeep Kamra, Utkarsh Agrawal, and Wolfgang Belzig, Noninteger-spin magnonic excitations in untextured magnets, Phys. Rev. B **96**, 020411(R) (2017).

[88] Sanchar Sharma, Victor A. S. V. Bittencourt, Alexy D. Karenowska, and Silvia Viola Kusminskiy, Spin cat states in ferromagnetic insulators, Phys. Rev. B **103**, L100403 (2021).

[89] Feng-Xiao Sun, Sha-Sha Zheng, Yang Xiao, Qihuang Gong, Qiongyi He, and Ke Xia, Remote generation of magnon Schrödinger cat state via magnon-photon entanglement, Phys. Rev. Lett. **127**, 087203 (2021).

[90] Shiwen He, Xuanxuan Xin, Feng-Yang Zhang, and Chong Li, Generation of a Schrödinger cat state in a hybrid ferromagnet-superconductor system, Phys. Rev. A **107**, 023709 (2023).

[91] Gerhard Kirchmair, Brian Vlastakis, Zaki Leghtas, Simon E. Nigg, Hanhee Paik, Eran Ginossar, Mazyar Mirrahimi, Luigi Frunzio, Steven M. Girvin, and Robert J. Schoelkopf, Observation of quantum state collapse and revival due to the single-photon Kerr effect, Nature **495**, 205 (2013).

[92] Z. Leghtas, S. Touzard, I. M. Pop, A. Kou, B. Vlastakis, A. Petrenko, K. M. Sliwa, A. Narla, S. Shankar, M. J. Hatridge, M. Reagor, L. Frunzio, R. J. Schoelkopf, M. Mirrahimi, and M. H. Devoret, Confining the state of light to a quantum manifold by engineered two-photon loss, Science **347**, 853 (2015).

[93] Andrei Vrajitoarea, Ziwen Huang, Peter Groszkowski, Jens Koch, and Andrew A. Houck, Quantum control of an oscillator using a stimulated Josephson nonlinearity, Nat. Phys. **16**, 211 (2020).

[94] Omar Gamel and Daniel F. V. James, Time-averaged quantum dynamics and the validity of the effective Hamiltonian model, Phys. Rev. A **82**, 052106 (2010).

[95] Wenjun Shao, Chunfeng Wu, and Xun-Li Feng, Generalized James' effective Hamiltonian method, Phys. Rev. A **95**, 032124 (2017).

[96] C. Gerry and P. Knight, *Introductory Quantum Optics* (Cambridge University Press, Cambridge, U.K., 2004).

[97] Alexandre Blais, Arne L. Grimsmo, S. M. Girvin, and Andreas Wallraff, Circuit quantum electrodynamics, Rev. Mod. Phys. **93**, 025005 (2021).

[98] J. W. Rao, Bimu Yao, C. Y. Wang, C. Zhang, Tao Yu, and Wei Lu, Unveiling a pump-induced magnon mode via its strong interaction with walker modes, Phys. Rev. Lett. **130**, 046705 (2023).

[99] Chao Zhang, Jinwei Rao, C. Y. Wang, Z. J. Chen, K. X. Zhao, Bimu Yao, Xu-Guang Xu, and Wei Lu, Control of magnon-polariton hybridization with a microwave pump, Phys. Rev. Appl. **20**, 024074 (2023).

[100] Maria Fuwa, Stable magnetic levitation of soft ferromagnets for macroscopic quantum mechanics, Phys. Rev. A **108**, 023523 (2023).